ICARUS 117, 120–127 (1995)

Mars Boundary Layer Modeling: Diurnal Moisture Cycle and Soil Properties at the Viking Lander 1 Site

HANNU SAVIJÄRVI

Department of Meteorology, University of Helsinki, Finland
E-mail: hannu.savijarvi@helsinki.fi

Received January 31, 1995; revised May 15, 1995

A dusty and moist martian atmospheric boundary layer model was augmented with a soil temperature diffusion scheme, simple soil hydrology, and interactive icecloud physics. It was applied to the summertime conditions at the Viking Lander 1 site (48°W, 22.5°N). A good simulation of the observed 1.6-m diurnal VL-1 temperature cycle was obtained when the soil properties were adjusted to that of a dryish at least 7-cm-thick sandlike topsoil layer with water availability of 0.05%, thermal conductivity of 0.18 W m^{-1} K^{-1}, and volumetric heat capacity of 0.8×10^6 J m^{-3} K^{-1}.

The cold nighttime temperatures lead to saturation of water vapor and surface fog formation in the model. The radiation fog extended to 60–80-m altitudes during the night, but remained thin, with maximum ice content of 0.05 g m^{-3} at 1.6 m height and vertical ice-waterpath of 0.43 precipitable (pr) μm by 07 LT. The fog dispersed within two hours after sunrise. The column water vapor amount stayed at about 16 pr μm (close to the Viking MAWD observations), being well mixed in the lowest 3 km with mixing ratios of about 0.18 g/kg, except near the surface where the ground sublimation/frosting and the condensation/sublimation into/from fog created a clear diurnal cycle. The 1.6-m relative humidities hit 100% at night (22–07 LT) but dropped below 1% in the afternoon.

1. INTRODUCTION

The topsoil thermal inertia of Mars is usually obtained by fitting remotely sensed surface temperatures with thermal model results. The thermal models have included a simple soil part and a simple atmospheric part, and the orbiter-sensed temperatures contain various error sources (e.g., due to uncertain atmospheric attenuation, spectral representativeness of the narrow-band observations, low diurnal sampling frequency). These estimations have been reviewed by, e.g., Haberle and Jakosky (1991).

In this article the 1-dimensional version of the atmospheric mesoscale model of Mars, developed at the University of Helsinki, is combined with a numerically fairly accurate thermal diffusion scheme for the soil. This model (equipped with a simpler force-restore soil scheme) has given good simulations of local winds and temperatures as validated by the Viking summertime observations (Savijärvi 1991b, Savijärvi and Siili 1993). Thus the atmospheric forcing of the surface heat budget should be reasonable. The two important soil thermal properties, conductivity and volumetric heat capacity, are here found by adjusting the model-predicted 1.6-m diurnal air temperatures to the relatively accurate Viking Lander 1 (VL-1) direct temperature observations. Thus both the thermal model and the observations for the fit should be of good quality.

Although the atmospheric moisture content has also been a variable in the model from the beginning and is included interactively in its radiation and surface schemes, our martian moisture results have not been published yet, since there is no direct quantitative verification. However, some other moisture calculations are beginning to be available for comparison (e.g., Zent *et al.* 1993). There are also plans to equip future Mars surface weather stations with humidity sensors. The Vaisala Ltd. Humicaps, for instance, are being tested for that purpose in the Finnish Meteorological Institute. It is obviously important for the mission instrumentation work to get some idea of what conditions are to be expected. Finally, although the moisture cycle does not have any large feedback on temperatures on Mars, the reverse is true. The frequent nighttime fogging and frosting around (and of) the VL cameras gave indirect evidence of the local diurnal water cycle (e.g., Pollack et al. 1977).

The 1-D model is here provided with a simple but proven bare-soil hydrology, similar to the 1980s GCMs of the Earth, and is constrained to produce the typical orbiter-observed atmospheric water vapor amounts. The resulting diurnal hydrologic cycle of sublimation, vertical diffusion, radiation fog formation, and frosting in the ground is described for summertime conditions at the VL-1 site (48°W, 22.5°N). The prevailing summertime tradewinds at this site produce realistic windspeeds in the model near the surface (necessary for realistic turbulence effects) even without local slope winds, which the 1-D model does not produce.

The major new findings of this paper are thus the alter-

0019-1035/95 $12.00

native approach to find the soil thermal properties and the consistent and quantitative description of the diurnal hydrologic cycle with ground fog formation.

2. MODEL DESCRIPTION

The 1-D column model is described in detail in Savijärvi (1991b), except for the present moisture and soil scheme additions. These and the important Monin–Obukhov surface layer scheme are described in detail below. The model variables are the horizontal wind ($\mathbf{V}$) components u, v, specific humidity q, and potential temperature $\Theta = T(p_{ref}/p)^{\kappa}$, where T is temperature, p_{ref} is a constant (here the mean surface pressure of 7.65 mb), and $\kappa = R/c_p = 0.251$. Pressure p at each fixed height is calculated hydrostatically from the predicted temperature profile. Dynamics also includes the Coriolis force, and a fixed large-scale pressure gradient force, given as geostrophic low-level tradewind of 10 m sec^{-1} in the present VL-1 summertime experiments. Vertical diffusion is based on a second-order closure (mixing length approach with the diffusion coefficients depending on windshear and hydrostatic stability). Thermal radiation is handled by an emissivity scheme for CO_2 tuned by a narrowband reference scheme, plus interactive water vapor (Savijärvi 1991a). Solar radiation is attenuated by absorption (CO_2 and dust), and by multiple scattering from dust.

Specific humidity q is a predicted variable in the model. Its local rate is changed at an atmospheric gridpoint by vertical diffusion and by condensation/sublimation onto/from iceparticles (i.e., fog/cloud). There are 20 vertical gridpoints (1.6, 7, 39, 85, 172 m, . . . , 20 km), and a 1-min timestep is used. The model is started at midnight of a solar day (sol 1) in conditions corresponding to the first sols of the Viking Lander 1 on Mars: latitude 22.5°N, midsummer (L_s = 100°), surface roughness length (z_o) 1 cm, albedo 0.24, V_g 10 m sec^{-1}, dust optical depth 0.3, initial surface temperature and pressure 225 K and 7.65 mb, and initial lapse rate 2 K/km. The results shown are for the second sol, after which the model more or less repeats itself. The present results are additional to those in Savijärvi (1991b) and in Savijärvi and Siili (1993).

2.1. Surface Layer Treatment

Surface fluxes of momentum, sensible heat, and latent heat are determined in the model by the bulk aerodynamic formulas

$$\tau = \rho C_d |\mathbf{V}| \mathbf{V} \tag{1}$$

$$H = \rho c_p C_h |\mathbf{V}| (T_o - T) \tag{2}$$

$$\mathrm{LE} = \rho L C_e |\mathbf{V}| (q_{sat}(T_o, p_o) - q)\beta, \tag{3}$$

where subindex o refers to the surface and T, p, q, $\mathbf{V}$, and density ρ (= p/RT) are from the lowest model level z_a at 1.6 m. c_p (736 J kg^{-1} K^{-1}) is specific heat of CO_2 at constant pressure, L (2.84 × 10^6 J kg^{-1}) latent heat of sublimation for water vapor, and β the topsoil moisture availability. The transfer ("drag") coefficient for momentum is $C_d = (k/\ln(z_a/z_o))^2 \cdot f(\mathrm{Ri})$, where k is the von Karman constant (0.4), and z_o is the roughness length. The transfer coefficients for heat and moisture C_h and C_e are set equal to C_d in neutral stability conditions. Ri is the Richardson number ($g/\Theta \cdot \partial\Theta/\partial z \; |\partial \mathbf{V}/\partial z|^{-2}$) of the lowest layer. The stability functions f(Ri) are based on similarity theory and mast measurements over smooth and homogeneous land sites on Earth. They are given by

unstable case, Ri < 0: $f(\mathrm{Ri}) = (1 - 16\ \mathrm{Ri})^{1/2}$ for momentum, $(1 - 64\ \mathrm{Ri})^{1/2}$ for heat, moisture

stable case, Ri > 0: $f(\mathrm{Ri}) = \max(0.05, 1 - 5\ \mathrm{Ri})$ for momentum, heat, and moisture.

Since the results with these formulations are quite reasonable both for the Earth (Savijärvi 1991c) and for Mars (Savijärvi 1991b, Savijärvi and Siili 1993, and the present results), similarity theory seems to be extendable to Mars, as was suggested by Sutton *et al.* (1978). One reason for the good results may be that the Viking sites look quite smooth and homogeneous in the VL camera pictures and from orbit.

2.2. Saturation of Moisture; Cloud Physics

The cold night temperatures near the ground may cause saturation of humidity, i.e., radiation fog formation. The saturation pressure curve $e_s(T)$ of water vapor over ice, representative of the cold temperatures and small ambient pressures on Mars, is taken from Buck (1981, Eq. (8)). Saturation specific humidity is calculated from $q_{sat} = m_w/m_c \cdot e_s/(p - (1 - m_w/m_c \cdot e_s))$, where m_w and m_c are the molecular weights of water vapor and CO_2 (18 and 44, respectively). After each timestep relative humidity RH (= q/q_{sat}) is checked at each gridpoint. Vapor amounts Δq in excess of 100% RH are removed into fog/ice, and the latent heat of condensation $L\Delta q/c_p$ is added to the air, as in Earth weather forecast models (e.g., Haltiner and Williams 1980). Since there are many condensation nuclei (dust particles) near the ground in Mars, immediate heterogeneous condensation at 100.0% RH is assumed. The fog so created sublimates back to vapor under subsaturated conditions (when temperatures rise in the morning), with q kept at q_{sat} until all fog has evaporated. The nighttime fog layer remains very thin even without any precipitation (snowfall). Precipitation is not assumed for reasons discussed later. The ice particle size distribution is not explicitly handled.

Even if the fog is thin, its thermal radiation may feed

back to its evolution; e.g. cooling by outradiation from the top of the fog layer may further increase the fog depth. The emissivity of the fog/ice was therefore included in the radiation scheme as a function of the predicted ice amount, as will be described later in detail.

2.3. *Initialization of Humidity and Handling of Soil Moisture*

The only relatively well-known quantitative humidity information about the Viking sites is the column amount of water vapor in the air, mapped by orbiters. At the VL-1 latitude in summertime, this value is typically 14–18 precipitable μm, and it does not seem to vary rapidly from sol to sol (Jakosky and Haberle 1992). This information was used for initializing and adjusting the moisture behavior in the model as follows.

The q profile was initialized for the VL-1 experiments by fixing the initial relative humidity of the air at each height to a value, which produced about 16 μm of column precipitable water ($\int_0^{p_s} q\, dp/g$), as observed. This initial RH value proved to be 10%. The moisture availability ("wetness") of the topsoil β was then fixed to a value, which kept the atmospheric total precipitable water content at about 16 μm during time integration over several sols. Thus the soil hydrology is very simple: β is conserved in the diurnally active topsoil (a centimeter or so) in these short integrations, while the measurable variable, the atmospheric vapor content, is approximately conserved, as observed. The suitable topsoil water availability β turned out to be 0.0005, giving 0.7–0.8 kg of condensed H_2O in a cubic meter of soil when using the estimated soil density of 1400–1600 kg m^{-3} of the VL sites. The same value was obtained in Zent *et al.* (1993) with a more complex approach, which is encouraging. The soil is thus fairly dry, as can perhaps be expected.

2.4. *Soil Temperature Prediction*

The ground surface temperature prediction was initially made in the model with a force-restore scheme similar to that used in the Mars GCM of Pollack *et al.* (1981). This gave a fairly good simulation of the diurnal temperature cycle at the VL-1 site (see Fig. 1 in Savijärvi 1991b). However, the gradual decrease of temperature late at night and the very rapid increase after sunrise were slightly slow in those integrations when compared to the VL observations. These deficits were shown in Savijärvi (1992) to be mostly due to the force-restore scheme, which is accurate for purely diurnal forcing, but distorts all harmonics (see Fig. 1). Thus in the present experiments, the soil temperature diffusion equation

$$\rho c\, \partial T/\partial t = \partial(\lambda \partial T/\partial z)/\partial z \qquad (4)$$

is numerically solved at five levels within the ground (z = 0, −0.006, −0.012, −0.045, −0.13 m), using the implicit Crank-Nicholson scheme as described in Savijärvi (1992). In (4), λ is thermal conductivity and ρc volumetric heat capacity of the soil. (The five levels were chosen so as to minimize numerical amplitude and phase errors when using soil properties typical for the VL sites). The diffusion equation (4) is forced from the top: energy flow into the ground $-\lambda \partial T/\partial z$ equals the net atmospheric energy input $G(t) = R_{net} - H - LE$ at the surface, while deep in the ground the energy flow is zero with the deep temperature set to constant (205 K).

Figure 1 shows the amplitude ratios and phase errors in the surface temperature response as a function of forcing frequency for three schemes: the five-level Crank-Nicholson scheme (CN5), the force-restore scheme, and the three-layer soil scheme of the ECMWF operational forecast model (1992 vintage), which is also used in the operational Nordic high-resolution limited area weather forecast model (HIRLAM). All three schemes are forced with the same prescribed sinusoidal surface energy input $G(t)$, use the same $\lambda = 0.18$ W m^{-1} K^{-1} and $\rho c = 0.8 \times 10^6$ J m^{-3} K^{-1}, valid for the VL-1 site, and the same 1-min timestep. All schemes can be seen to be accurate for the diurnal frequency, but only the CN5 scheme can adequately manage the full range of forcing frequencies. This is important as in reality $G(t)$ is nonsinusoidal and thus includes many frequencies simultaneously. Thus the soil diffusion scheme chosen appears to be numerically fairly accurate for its purpose.

3. RESULTS: SURFACE AND SOIL THERMAL PROPERTIES AT THE VIKING LANDER 1 SITE

In the present experiments, the soil albedo is fixed to the observed visual albedo 0.24 of the VL-1 site, but the unknown thermal properties λ and ρc (initially constant in depth and time) were adjusted (by trial and error) so as to get the best overall agreement with the observed diurnal air temperature cycle near the surface. The moisture cycle, described in Section 4, was also present in the model. Figure 2 shows the 0–3-sol averaged temperature observations from Hess *et al.* (1976), and the best-fit model results for sol 2. The simulation is impressively good, both for the ground temperatures and for the 1.6-m VL-1 air temperatures. Note specifically the temperature response just before and after sunrise, which is now well handled by the model. The "afternoon cooling" problem (modeled temperatures too high in the afternoon), typical in many previous thermal models of Mars (Haberle and Jakosky 1991), is absent in Fig. 2: The afternoon air temperatures are as well simulated as the rest of the day.

The best-fit soil thermal properties proved to be equivalent to their combination, which appeared in the force-restore scheme in Savijärvi (1991b). This is also encouraging

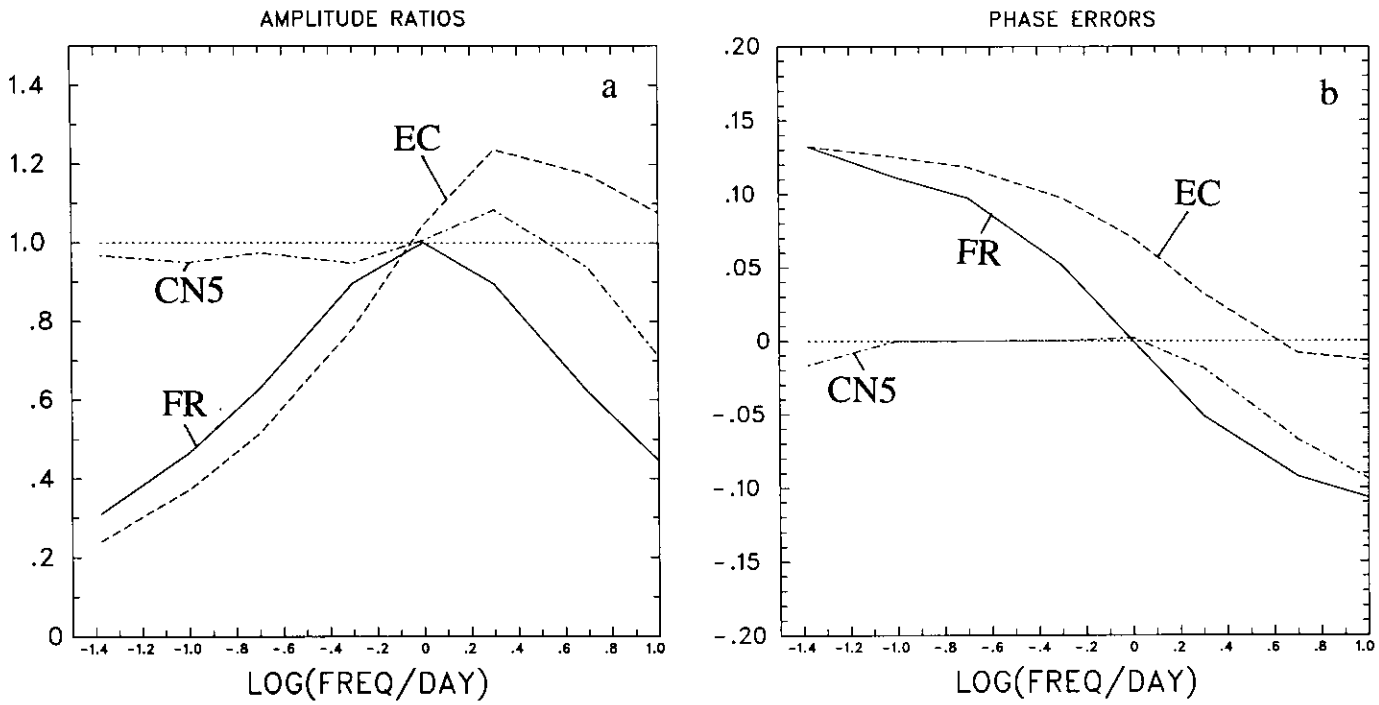

FIG. 1. (a) Amplitude response ratios (simulated amplitude/exact amplitude) of the sinusoidally top-forced soil temperature diffusion equation when numerically solved with the Crank-Nicholson 5-level scheme (CN5), force-restore scheme (FR), and the ECMWF-HIRLAM scheme (EC), for constant soil thermal properties appropriate for Mars. Timestep is 60 sec in all three schemes. Values < 1 mean amplitude underestimation in the numerical solution. (b) Same as (a) but for phase errors (differences to the exact phase; 0.1 = 36°). Positive/negative values mean maxima and minima occurring too late/early in the numerical solution.

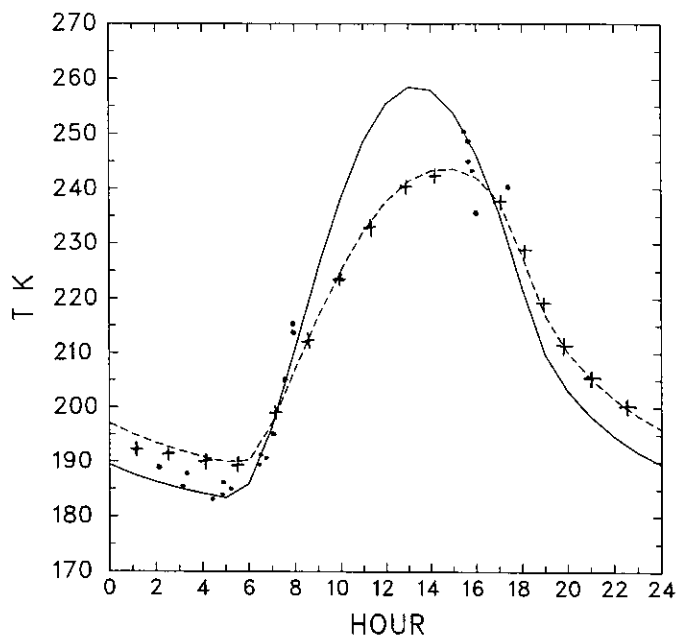

FIG. 2. The VL-1 model ground (solid line) and 1.6-m (dashed line) diurnal temperature cycle for sol 2, and the 1.6-m VL-1 temperatures averaged over sols 0–3 (+). Some remotely sensed ground temperatures are also shown (●). (Observations from Hess *et al.* 1976).

and indicates some robustness. The best-fit values are thermal conductivity $\lambda = 0.18\ \mathrm{W\ m^{-1}\ K^{-1}}$, and volumetric heat capacity $\rho c = 0.8 \times 10^6\ \mathrm{J\ m^{-3}\ K^{-1}}$. The indicated thermal inertia $I = (\lambda \rho c)^{1/2}$ of the VL-1 site topsoil is thus 380 SI units ($\mathrm{W\ m^{-2}\ s^{1/2}\ K^{-1}}$). This is more than was obtained by Haberle and Jakosky (1991), who matched ground temperatures without fixing the albedo. They ended up with I = 215 SI units but with a slightly high albedo of 0.32. The remotely sensed IRTM ground temperatures used by Haberle and Jakosky (1991) represent large area averages. This may partly explain the difference since the present values are really spot values for the VL-1 site.

The thermal properties are typical for dryish sandlike material. The values indicate medium-to-coarse sand with particle size around 500 μm, judging from Haberle and Jakosky (1991, Fig. 15) and from Edgett and Christensen (1991, Fig. 2). Rocky sand was, of course, seen around the Viking landers in the VL camera pictures and its dryness has been indicated, e.g., by spectral measurements from orbit (e.g., Söderblom 1992).

Some sensitivity tests were made by varying the values of λ and ρc independently but keeping everything else the same in the simulations. It appeared, as expected, that the thermal inertia I controlled the temperature extrema, high (low) inertias producing small (strong) diurnal extrema. However, the *shape* of the temperature curve was

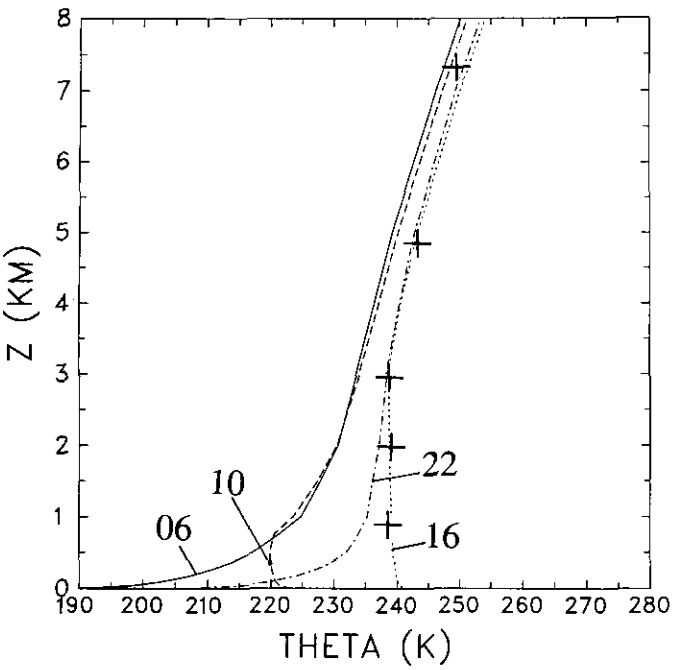

FIG. 3. The potential temperature profiles $\Theta(z)$ at 06, 10, 16, and 22 LT during sol 2 in the VL-1 model, and the VL-1 entry descent sounding at about 16 LT (+; data from Seiff and Kirk 1977).

controlled by λ: small (large) λ, for the same I and thus for the same temperature extrema, gives quick (slow) surface cooling in the afternoon. Thus thermal inertia alone is not enough to specify uniquely the soil thermal properties (of a Mars GCM, for instance). Rather, the two properties, λ and ρc, are both needed. Several ground temperature measurements from orbit during the day, a few preferably in the afternoon, may be used to map the two properties simultaneously.

Some attempts were made where rocklike layers (i.e., large λ and ρc) were set below the topmost sandlike layers in the multilevel soil scheme. These experiments failed to give any fit to the observed temperatures better than that in Fig. 2. Thus it appears that the sandlike layer was at least 7–10 cm thick at the VL-1 site during the observing conditions in 1976. There may be rock deeper below, but its effect does not enter into the fast diurnal time scale.

4. RESULTS: DIURNAL MOISTURE AND FOG CYCLE AT VL-1 IN SUMMER

Figure 3 shows the potential temperature profiles $\Theta(z)$ at 06, 10, 16, and 22 hours local time (LT) at the VL-1 site during sol 2 of the simulation. The observed VL-1 entry sounding, at about 16 LT, is also shown. A good correspondence to the model result can be seen. The very steep surface night inversion at 06 LT changes to a rapidly growing well-mixed layer during the morning. The mixed layer is about 600 m high at 10 LT, extends to 3 km by 16 LT, and collapses soon after sunset. The relative roles of turbulence and radiation in the evolution of the diurnal temperature variation were described in Savijärvi (1991b) and in Haberle *et al.* (1993).

The model-predicted specific humidity profiles $q(z)$ at 06, 10, 16, and 22 LT during sol 2 are shown in Fig. 4. High up above the boundary layer diurnal variation is small in q, and the profiles remain at their initial values, defined by the initial 10% RH level. In the upper boundary layer (1–3-km altitudes) the q-values are well mixed throughout the day. However, near the ground the cold temperatures at night (Figs. 2, 3) lead to saturation. Excess moisture is condensed into fog-ice and there is also some frost loss into the ground. Thus at 06 LT there is less water vapor near the ground. Soon after sunrise temperatures start to rise rapidly and the then-existing thin shallow fog sublimates back to vapor in the subsaturated environment. The strong turbulence over the "hot" surface in the morning can be seen in the 10 LT q profile, with mixing and entrainment from the more moist upper boundary layer into the lowest well-mixed 600 m. Sublimation from the surface also replenishes the moisture field at daytime. Thus the column water vapor amount stays at about 16 pr μm throughout the day. The typical boundary layer values of absolute humidity q are about 1.8×10^{-4}, or 0.18 g/kg, according to Fig. 4.

The relative humidity and the accumulated fog amount, i.e., mixing ratio of ice, assuming no precipitation (no snowfall), are shown for the lowest model levels in Table

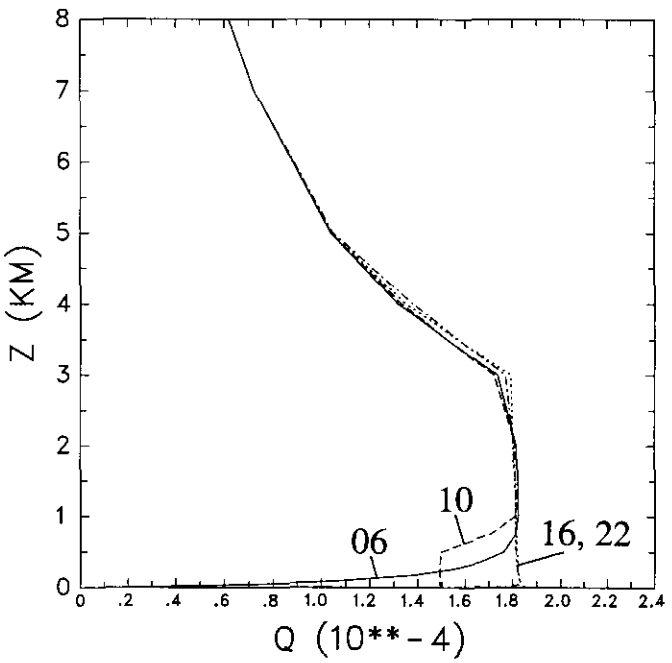

FIG. 4. The VL-1 model specific humidity profiles $q(z)$ at 06, 10, 16, and 22 LT during sol 2.

TABLE I

The Relative Humidity (in Percent), and Cumulated Fog Amount (Mixing Ratio of Ice, in 0.1 g/kg or 10^{-4}) in the Lowest Model Gridpoints during the Night Hours in the VL-1 Experiment

	Relative humidity (%)					Mixing ratio of ice (10^{-4})		
Hour	z (m) 1.6	7	39	85	172	z (m) 1.6	7	39
21	66	38	15	9	6			
22	100	63	25	14	8	0.09		
23	100	76	35	21	12	0.17		
24	100	89	45	28	16	4.80		
01	100	100	60	39	23	10.81	0.01	
02	100	100	72	48	30	15.41	0.55	
03	100	100	87	60	37	18.77	1.46	
04	100	100	100	72	45	21.26	2.51	0.07
05	100	100	100	83	54	23.09	3.40	0.49
06	100	100	100	93	63	24.38	4.06	1.05
07	100	100	99	88	64	25.01	4.40	
08	40	44	47	50	51			
09	14	17	20	21	23			

I for nighttime. The rapid increase of relative humidity in the evening, due to the falling temperatures, leads to saturation and fog formation at around 22 LT near the ground. The depth of the fog layer increases slowly from about 5 m at midnight to about 60–80 m just after sunrise (06 LT), after which the fog layer disintegrates rapidly from top down. It is gone within two hours from sunrise (this is typical for Earth radiation fogs, too). The fog is quite thin even in the lowest 1.6-m level, where the mixing ratio of ice reaches 2.5 g/kg by 07 LT. This transfers to 0.052 g of ice particles in a cubic meter of air. (The observed ice contents in the Earth's cirrus clouds are similar, e.g., Heymsfield 1975). During the morning hours, temperatures start to rise and the relative humidity falls rapidly near the surface. This strong repetitive diurnal variation of relative humidity (see also Table II), and the frequent saturation (fogging and frosting at night), sets great demands for the humidity measuring systems of future weather stations on Mars, if they are based on RH measurements.

Some 1.6-m model values (wind speed, relative humidity), surface energy fluxes (net radiation, net solar radiation, downcoming thermal radiation, H, and LE), and the column water vapor and ice particle amounts are shown in Table II for each hour of sol 2 in the VL-1 simulation. The wind speeds are close to those observed at VL-1, being 4–6 m/sec in the daytime and 1-3 m/sec at night. The model's sensible heat flux H at midday (about 10 W m^{-2}) is also close to the only independent estimate: that from the observed temperature variation at VL-1 in Sutton *et al.* (1978).

For the latent heat flux LE, there is unfortunately no observed estimate. LE is clearly unimportant in the surface heat budget, being only 0.1 W m^{-2} at 13 LT, but it shows a typical diurnal cycle with small negative values (i.e., weak frost formation) at night and sublimation during the day. The column precipitable water vapor amount hovers around 16 pr μm, decreasing slightly during the night (due to loss into fog and groundfrost) and increasing again during the day (by sublimation from fog and ground). The precipitable ice amount of the column is small in comparison. It is only 0.43 μm at its maximum just before the fog dispersal at 07 LT. The morning thickening of radiation fogs just before their dispersal, typical on Earth, is indicated also on Mars by the model results.

The maximum vertical ice-waterpath IWP of the fog layer is 0.43 pr μm = 0.43 g m^{-2}. This is too little to exhibit strong radiative effects. The thermal emissivity parameterization in our model, developed for the Earth's iceclouds ($\varepsilon_{ice} = 1 - \exp(-0.06 \cdot \mathrm{IWP})$, Ebert and Curry 1992), gives ε_{ice} of 1.5% for the whole fog layer, which is much less than the typical 15% emissivity of a clear air column on Mars (e.g., Leovy 1985). An icecloud this thin is also practically transparent to solar radiation (Ebert and Curry 1992). The effect of the fog on solar radiation was therefore neglected. The fog was kept thin primarily by the wind and the subsequent turbulent mixing; with less wind the fog might have grown thicker with clearer signal in the temperature profile.

Figure 5 shows the instantaneous sublimation/condensation rate at the surface (E, i.e., (3) divided by L), and the ice amount in the atmosphere ("precipitation rate" P) during sol 2 in the simulation. Both are given in units of μm/day. The sublimated positive daytime amounts of E are much higher than those condensed (negative E) at night. The precipitable ice amount P is not enough to

TABLE II

The 1.6-m Windspeed V and Relative Humidity RH, the Surface Net Radiation R_{net}, Net Solar Radiation S_{net}, Downcoming Longwave Radiation DLW, H, LE, the Precipitable Water Vapor Content PWC, and Ice Particle Content IPC in the VL-1 Simulation during sol 2

Hour	V (m/sec)	RH (%)	R_{net} (W m^{-2})	S_{net} (W m^{-2})	DLW (W m^{-2})	H (W m^{-2})	LE (mW m^{-2})	PWC (μm)	IPC (μm)
1	2.72	100.00	−51.59	0.00	22.08	−1.29	−0.01	16.11	0.08
2	2.78	100.00	−49.30	0.00	21.59	−1.23	−0.01	16.05	0.14
3	2.84	100.00	−47.44	0.00	21.17	−1.16	−0.01	15.99	0.19
4	2.88	100.00	−45.92	0.00	20.79	−1.08	0.00	15.94	0.25
5	2.92	100.00	−44.63	0.00	20.50	−0.99	0.00	15.86	0.32
6	2.81	100.00	−11.04	36.62	20.43	−0.60	0.00	15.79	0.39
7	2.89	100.00	54.14	116.99	21.19	0.51	0.01	15.76	0.43
8	4.48	40.13	109.32	198.20	21.46	1.65	0.26	15.76	0.00
9	5.37	14.30	148.73	268.81	23.58	4.58	2.50	15.76	0.00
10	5.80	5.78	169.73	323.06	25.92	7.57	12.34	15.77	0.00
11	5.92	2.82	173.48	357.10	28.28	9.52	37.59	15.81	0.00
12	5.78	1.63	162.47	368.61	30.41	10.15	75.58	15.89	0.00
13	5.68	1.15	139.43	356.82	32.12	9.60	104.56	16.01	0.00
14	5.56	0.95	106.78	322.52	33.24	7.98	98.14	16.15	0.00
15	5.29	0.90	66.54	268.04	33.84	5.25	61.33	16.24	0.00
16	5.01	1.00	20.51	197.26	33.75	2.10	25.60	16.28	0.00
17	3.73	1.51	−28.94	115.97	32.92	−0.45	5.64	16.30	0.00
18	2.01	4.46	−75.40	35.75	30.89	−0.74	0.59	16.30	0.00
19	1.85	15.34	−86.43	0.00	28.62	−1.03	0.10	16.30	0.00
20	1.87	35.04	−75.09	0.00	26.92	−1.14	0.01	16.30	0.00
21	1.92	66.16	−67.71	0.00	25.60	−1.24	−0.03	16.30	0.00
22	1.97	100.00	−62.20	0.00	24.51	−1.33	−0.04	16.29	0.00
23	2.04	100.00	−57.90	0.00	23.59	−1.41	−0.03	16.26	0.00
24	2.09	100.00	−54.41	0.00	22.88	−1.41	−0.02	16.22	0.03

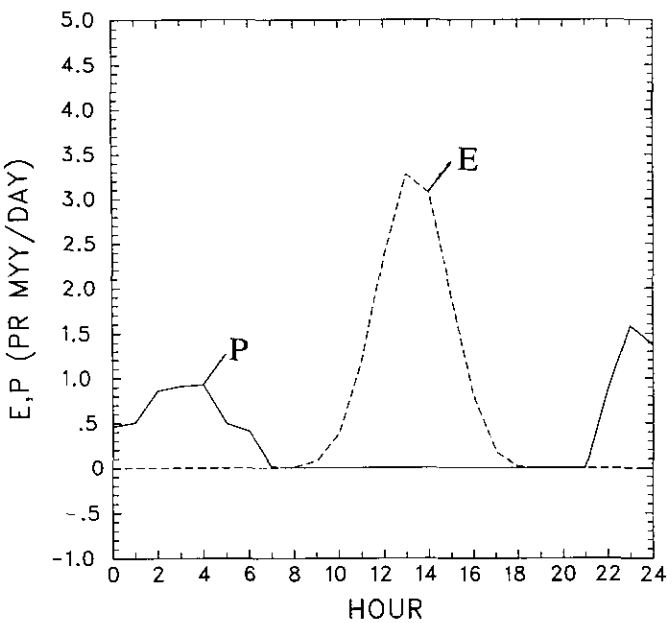

FIG. 5. Surface sublimation/condensation rate E and the ice particle column content (precipitable rate P), in pr μm/sol, during sol 2 in the VL-1 simulation.

balance the surface ice budget even if all of it precipitated to the surface. Both aspects are perhaps natural during midsummer at the low latitude of 22°N.

How much of the fog really precipitates to the surface is not known. This must depend on the dust particle size spectrum and how effectively the martian dust particles act as condensation nucleii for water-ice under supersaturation. Some Viking camera pictures from summer mornings have indicated white spots in shadows, but whether this is frost or snow is not known. However, since the temperatures are very cold at night (well below −40°C), it is likely that supercooled water droplets do not exist and do not produce ice crystals rapidly. This Bergeron–Findeisen precipitation process, common in the Earth's mixed (ice-water) clouds, therefore does not operate in all likelihood. The fog is also very thin so that growth by diffusion and the coalescence–collition processes may also be slow and ineffective. Thus snowfall is unlikely. The present calculations have therefore assumed no precipitation.

5. SUMMARY AND CONCLUDING REMARKS

The 1-D version of a dusty and moist Mars mesoscale model was augmented with a numerically accurate soil

temperature diffusion scheme (Fig. 1), a simple bare soil hydrology scheme, and an atmospheric cloud physics scheme (removal of water vapor supersaturation into ice; ice sublimation to vapor; cloud emissivity dependent on the predicted ice particle content). This fairly complete thermal atmospheric boundary layer–topsoil model was then applied to the summertime conditions at the VL-1 site with surface albedo fixed to 0.24 and roughness length to 1 cm. An impressively good simulation of the observed VL-1 diurnal temperature cycle (Fig. 2) was obtained when the ground was adjusted to a dryish sandlike material with water availability ("wetness") of 0.0005 (0.7–0.8 kg m^{-3}), thermal conductivity of 0.18 W m^{-1} K^{-1}, and volumetric heat capacity of 0.8×10^6 J m^{-3} K^{-1}. At least the top 7–10 cm appeared to be sandlike in the VL-1 site (in 1976). The simulated diurnal hydrologic cycle showed:

—sublimation of moisture from the ground and strong mixing of vapor in the growing well-mixed boundary layer during the morning and midday

—well-mixed absolute humidity profile and very low relative humidities in the afternoon (<1%)

—rapid increase of relative humidity in the evening with radiation fog formation at about 22 LT

—loss of water vapor to ice (fog), and into frost formation at the ground during the night

—the thin fog was thickest near the ground with ice mixing ratios of up to 2.5 g/kg

—foglayer grew to 60–80-m heights and dispersed in less than two hours after sunrise.

The typical mixing ratios of water vapor were around 0.18 g/kg in the well-mixed boundary layer, and the column water vapor amount stayed at around 16 pr μm throughout the integration, as observed. There is no other direct quantitative verification of moisture (or fog) near the surface of Mars yet, but the VL cameras, and those on orbiters, have recorded fogging and frosting during summer nights.

The model-produced martian fog properties resemble those observed in the Earth's radiation fogs, and the simulated ice particle contents ($\approx$0.05 g m^{-3} at maximum) are similar to those measured in the Earth's ice (cirrus) clouds. The soil properties obtained are close to other estimates for the VL-1 site. Thus the results look plausible. They form an internally consistent set of typical "local weather," which could occur and be observable on summertime Mars.

REFERENCES

Buck, A. L. 1981. New equations for computing vapor pressure and enhancement factor. *J. Appl. Meteor.* **20**, 1527–1532.

Ebert, E., and J. Curry 1992. A parameterization of ice cloud optical properties for climate models. *J. Geophys. Res.* **97**, 3831–3836.

Edgett, K. S., and P. R. Christensen 1991. The particle size of martian aeolian dunes. *J. Geophys. Res.* **96**, 22,765–22,776.

Haberle, R. M., and B. M. Jakosky 1991. Atmospheric effects on the remote determination of thermal inertia on Mars. *Icarus* **90**, 187–204.

Haberle, R. M., H. C. Houben, R. Hertenstein, and T. Herdtle 1993. A boundary layer model for Mars: Comparison with Viking lander and entry data. *J. Atmos. Sci.* **50**, 1544–1559.

Haltiner, G. J., and R. T. Williams 1980. *Numerical Prediction and Dynamic Meteorology*. Wiley, New York.

Hess, S. L., R. M. Henry, C. B. Leovy, J. A. Ryan, J. E. Tillman, T. E. Chamberlain, H. L. Cole, R. G. Sutton, G. C. Greene, W. L. Simon, and J. L. Mitchell 1976. Preliminary meteorological results on Mars from the Viking Lander 1. *Science* **193**, 788–791.

Heymsfield, A. J. 1975. Cirrus uncinus generating cells and the evolution of cirriform clouds, 1, Aircraft observations of the growth of the ice phase. *J. Atmos. Sci.* **32**, 799–808.

Jakosky, B. M., and R. M. Haberle 1992. The seasonal behavior of water on Mars. In *Mars*, pp. 969–1016. Univ. of Arizona Press, Tucson.

Leovy, C. B. 1985. The general circulation of Mars: Models and observations. *Adv. Geophys. A* **28**, 327–346.

Pollack, J. B., D. Colburn, R. Kahn, J. Hunter, W. van Kamp, C. E. Carlston, and M. R. Wolf 1977. Properties of aerosols in the martian atmosphere, as inferred from Viking lander imaging data. *J. Geophys. Res.* **82**, 4479–4496.

Pollack, J. B., C. B. Leovy, P. W. Greiman, and Y. Mintz 1981. A martian general circulation experiment with large topography. *J. Atmos. Sci.* **38**, 3–29.

Savijärvi, H. 1991a. Radiative fluxes on a dustfree Mars. *Contrib. Atmos. Phys.* **64**, 103–112.

Savijärvi, H. 1991b. A model study of the PBL structure on Mars and Earth. *Contrib. Atmos. Phys.* **64**, 219–229.

Savijärvi, H. 1991c. The U.S. Great Plains diurnal ABL variation and the nocturnal low-level jet. *Mon. Weather Rev.* **119**, 833–840.

Savijärvi, H. 1992. On surface temperature and moisture prediction in atmospheric models. *Contrib. Atmos. Phys.* **65**, 281–292.

Savijärvi, H., and T. Siili 1993. The martian slope winds and the nocturnal PBL jet. *J. Atmos. Sci.* **50**, 77–88.

Seiff, A., and D. B. Kirk 1977. Structure of the atmosphere of Mars in summer at mid-latitudes. *J. Geophys. Res.* **82**, 4364–4378.

Söderblom, L. A. 1992. The composition and mineralogy of the martian surface from spectroscopic observations: 0.3 μm to 50 μm. In *Mars*, pp. 557–593. Univ. of Arizona Press, Tucson.

Sutton, J. L., C. B. Leovy, and J. E. Tillman 1978. Diurnal variations of the martian surface layer meteorological parameters during the first 45 sols at two Viking lander sites. *J. Atmos. Sci.* **35**, 2346–2355.

Zent, A. P., R. M. Haberle, H. C. Houben, and B. M. Jakosky 1993. A coupled subsurface-boundary layer model of water on Mars. *J. Geophys. Res.* **98**, 3319–3337.